Curcumin-induced antitumor effects on triple-negative breast cancer patient-derived xenograft tumor mice through inhibiting salt-induced kinase-3 protein

Tzu-Chun Cheng [a,1], John Oliver Sayseng [b,1], Shih-Hsin Tu [c,d,e,1], Ting-Ching Juan [a], Chia-Lang Fang [f,g], You-Cheng Liao [h], Cheng-Ying Chu [i,j], Hui-Wen Chang [k], Yun Yen [i], Li-Ching Chen [i,*], Yuan-Soon Ho [a,h,i,k,**]

[a] School of Medical Laboratory Science and Biotechnology, College of Medical Science and Technology, Taipei Medical University, Taipei 110, Taiwan
[b] International Graduate Program in Medicine, College of Medicine, Taipei Medical University, Taipei 110, Taiwan
[c] Taipei Cancer Center, Taipei Medical University, Taipei 110, Taiwan
[d] Breast Medical Center, Taipei Medical University Hospital, Taipei 110, Taiwan
[e] Department of Surgery, School of Medicine, College of Medicine, Taipei Medical University, Taipei 110, Taiwan
[f] Department of Pathology, School of Medicine, College of Medicine, Taipei Medical University, Taipei 110, Taiwan
[g] Department of Pathology, Taipei Medical University Hospital, Taipei Medical University, Taipei 110, Taiwan
[h] Graduate Institute of Medical Sciences, College of Medicine, Taipei Medical University, Taipei 110, Taiwan
[i] TMU Research Center of Cancer Translational Medicine, Taipei Medical University; Taipei 110, Taiwan
[j] CRISPR Gene Targeting Core Lab, Taipei Medical University, Taipei 110, Taiwan
[k] Department of Medical Laboratory, Taipei Medical University Hospital, Taipei, Taiwan

Abstract

This study demonstrated for the first time that curcumin effectively inhibits the growth of triple-negative breast cancer (TNBC) tumors by inhibiting the expression of salt-induced kinase-3 (SIK3) protein in patient-derived xenografted tumor mice (TNBC-PDX). For TNBC patients, chemotherapy is the only option for postoperative adjuvant treatment. In this study, we detected the *SIK3* mRNA expression in paired-breast cancer tissues by qPCR analysis. The results revealed that *SIK3* mRNA expression was significantly higher in tumor tissues when compared to the normal adjacent tissues (73.25 times, n = 183). Thus, it is proposed for the first time that the antitumor effect induced by curcumin by targeting SIK3 can be used as a novel strategy for the therapy of TNBC tumors. *In vitro* mechanism studies have shown that curcumin (>25 μM) inhibits the SIK3-mediated cyclin D upregulation, thereby inhibiting the G1/S cell cycle and arresting TNBC (MDA-MB-231) cancer cell growth. The SIK3 overexpression was associated with increased mesenchymal markers (i.e., Vimentin, α-SMA, MMP3, and Twist) during epithelial−mesenchymal transition (EMT). Our results demonstrated that curcumin inhibits the SIK3-mediated EMT, effectively attenuating the tumor migration. For clinical indications, dietary nutrients (such as curcumin) as an adjuvant to chemotherapy should be helpful to TNBC patients because the current trend is to shrink the tumor with preoperative chemotherapy and then perform surgery. In addition, from the perspective of chemoprevention, curcumin has excellent clinical application value.

Keywords: Curcumin, Epithelial-mesenchymal transition, Patient-derived xenografted mice, Salt-induced kinase-3, Triple-negative breast cancer

Received 19 August 2021; revised 13 September 2021; accepted 22 September 2021.
Available online ■ ■ ■

* Corresponding author at: TMU Research Center of Cancer Translational Medicine, Taipei Medical University, No. 250, Wu-Xing St, Taipei. Taiwan.
** Corresponding author at: Graduate Institute of Neural Regenerative Medicine, College of Medical Science and Technology, Taipei Medical University, No. 250, Wu-Xing St, Taipei. Taiwan.
E-mail addresses: lcchen@tmu.edu.tw (L.-C. Chen), hoyuansn@tmu.edu.tw (Y.-S. Ho).
[1] The authors are contributed equally.

https://doi.org/10.38212/2224-6614.3387

1. Introduction

Breast cancer is the most common malignant tumor in women globally, and it is a heterogeneous disease. According to the expression of estrogen receptor (ER), progesterone receptor (PR), and human epidermal receptor 2 (HER2), breast cancer can be divided into three subtypes. 60%–70% of breast cancers are hormone receptor (HR) positive, characteristic of ER and/or PR expression. HER2-enriched breast cancer accounts for 13%–15% of all breast cancers and is characterized by the amplification of HER2 amplicons. 15% of breast cancers are triple-negative breast cancer (TNBC), characterized by a lack of ER, PR, and HER2 receptor expression [1]. Current clinical studies had shown that anti-endocrine and anti-HER2 drugs are very effective for HR-positive and HER2-enriched breast cancer treatment strategies. However, TNBC lacks a suitable therapeutic target, and chemotherapy is the primary treatment option for TNBC [2], and continued use of conventional cancer therapies can lead to chemotherapy resistance. Therefore, finding alternative therapies is essential to break this vicious cycle. The concept of combination therapy relies on two or more therapeutic agents and has been introduced into the development of cancer treatment. Over the years, natural compounds had a wide range of medicinal properties and have synergistic effects through combination therapy [3]. Natural compounds, such as inotilone, EGCG, curcumin, phloretin, garcinol, and resveratrol, are promising drug candidates for the prevention and treatment of breast cancer through multitargeting.

Curcumin is a hydrophobic polyphenol with biological activity, commonly known as turmeric (Curcumaceae), and is the main curcuminoid diferroyl methane. Curcumin is listed as a " Generally Recognized As Safe" compound by the US Food and Drug Administration (FDA), supporting patient safety and tolerability when consumed [3]. In addition, a large amount of preclinical evidence indicates that curcumin can block the growth of breast cancer by regulating multiple signaling pathways, inducing apoptosis, and inhibiting proliferation, survival, angiogenesis, and metastasis pathways [4]. Interestingly, curcumin supplementation reduced the adverse reactions caused by patients receiving conventional treatment [5–7]. These characteristics have significant advantages for developing curcumin combination therapy to treat cancer.

Continuous proliferation signals and avoidance of growth inhibition are typical characteristics of cancer cells [8]. Cyclin-dependent kinase (CDK) activity is usually dysregulated in cancer cells. Therefore, CDK has become an attractive target for anticancer therapy. The FDA approved the clinical application of CDK4/6 inhibitors Palbociclib, Ribociclib, and Abemaciclib [9]. Importantly, CDK4/6 inhibitor combined with hormone therapy has been successfully used as the standard first-line treatment for women with ER-positive breast cancer before and after menopause [10]. In addition, other dysregulated cell cycle regulatory proteins, such as tumor suppressor genes (p16, p21, p27, and p53) or oncogenes (cyclin A, B, C, D1, E) can be a target for future anticancer therapy [8]. Tumor suppressor p27 (Kip1) is an important regulator of cell cycle transition from G1 to S [11]. The p27-mediated cell cycle inhibition impedes the catalytic activity of cyclin D-, E–, A- and B-CDK complexes through the interaction of its N-terminal domain with cyclin and CDK subunit. Down-regulation of p27 is associated with high-grade breast cancer. Decreased p27 protein levels are also an indicator of poor clinical outcomes in most lymph node-negative breast cancer patients. In HR-positive cancers, lower p27Kip1 is associated with reduced overall survival (hazard ratio (HR) = 1.42; 95% confidence interval (CI) = 1.05 to 1.94; disease-free survival rate HR = 1.27; and 95% CI = 0.99 to 1.63), compared with cancers with higher p27Kip1 expression treated with adjuvant therapy (doxorubicin and cyclophosphamide) [12]. The above results indicate that p27 can be used as a prognostic and therapeutic significance.

Salt-induced kinase (SIK) belongs to the AMP-activated protein kinase (AMPK) family [13]. Its function is mainly related to physiological processes associated with energy response, such as gluconeogenesis and lipid metabolism [13]. SIK1 was initially isolated from the adrenal glands of rats on a high-salt diet [13]. Subsequent studies have shown that SIK2 and SIK3 are ubiquitous in humans and are mainly expressed in fat and nerve tissues, respectively [14]. In addition, these SIK family members are dysregulated in various cancers, including ovarian, breast, prostate, and lung cancers [15–18], indicating that SIK may be involved in its occurrence or tumor progression. SIK1 exerts a tumor suppressor effect and inhibits metastasis through p53-dependent anoikis [15]. However, SIK2 and SIK3 play carcinogenic effects in various cancers [13]. SIK2 directly phosphorylates p85 to activate AKT kinase activity [19] and is an essential

upstream regulator of ChREBP-induced steatosis [13]. SIK3 is a candidate oncogene that provides a survival advantage for the growth of cancer cells [16].

This study shows that SIK3 is highly expressed in TNBC and activates the G1/S cyclin D/CDK4 complex to promote cell growth. Our results first prove that curcumin effectively reduces tumor growth by reducing the level of SIK3 protein in the TNBC-PDX model. Second, our results show that dietary nutrients (such as curcumin) are helpful as an adjuvant to chemotherapy for TNBC patients. In addition, from the perspective of healthy people's daily health care and chemoprevention, curcumin has excellent clinical application value for cancer prevention.

2. Material and methods

2.1. Cell culture

Cell lines, SKBR3, BT474, AU565, HCC1937, BT-549, Hs-578T, MDA-MB-231, MDA-MB-436, MDA-MB-468, MDA-MB-453, MCF-7, T47D, ZR-75-1, and MCF-10A cells were obtained from the American Type Culture Collection (ATCC, Manassas, Virginia, USA) and had been thoroughly tested and certified by ATCC. The cells were maintained in DMEM/F12, supplemented with 10% heat-inactivated FBS and 50 U/mL PSN in a 5% CO_2 humidified incubator at 37 °C.

2.2. Human patient samples

All patient samples (n = 342) were collected at the Taipei Medical University Joint-Biobank following approval from the Taipei Medical University-Joint Institutional Review Boards (TMU-JIRB No. N202002005). The studies were conducted following recognized ethical guidelines. The clinical and pathological information of patient samples came from the Joint Biobank of Taipei Medical University.

2.3. Quantitative polymerase chain reaction (qPCR) analysis

RNA extraction, reverse transcription, and qPCR were performed according to the method described in our previous paper [20]. According to the manufacturer's protocol, qPCR was performed using the Roche LightCycler LC2.0 (Roche Molecular Biochemicals, Mannheim, Germany). The *SIK3* expression levels were calculated using the built-in software (Roche LightCycler Version 4.0) and normalized to endogenous *GUS* expression. The primers were listed in Table S1.

2.4. Wound-healing assay

Cells (231-WT, 231-Vc, 231-SIK3, 231-Sc, 231-Si, 231-Cas9 C, and 231-SIK3 KO) were seeded with 3.5×10^4 cells in each well (0.22 cm^2) of the μ-insert. The fixed distance of each μ-insert is 0.5 mm. Images were collected at 0 and 16 h using the Leica DMI 4000B Microscope Imaging System (Leica, Wetzlar, Germany). Use Image J software to measure enclosed areas. Repeated determinations in three independent experiments.

2.5. Colony-forming assay

Cells (231-WT, 231-Vc, 231-SIK3, 231-Sc, 231-Si, 231-Cas9 C, and 231-SIK3 KO) were seeded at 300 cells in a 3 cm Petri dish. After three weeks, the cells were fixed with 4% formaldehyde and stained with 0.05% crystal violet. The images were collected digitally and analyzed using Image J software. Repeated determinations in three independent experiments.

2.6. Immunofluorescence (IF) staining and förster resonance energy transfer (FRET)

According to the method described in our previous report [21], cells (SK-Vc, SK-SIK3, 231-Vc, and 231-SIK3) and FFPE sections (BC081116c, US Biomax, Inc., Rockville, MD, USA) were rehydrated and heated in Tris–EDTA buffer (pH 9.0) for 30 min. The samples were stained with primary antibodies (anti-cyclin D, anti-p27, and anti-CDK4 for cells; anti-p27 for FFPE sections) and incubated with the anti-rabbit FITC secondary antibody. The cells and FFPE sections were stained with the second primary antibody (anti-SIK3) and incubated with an anti-mouse rhodamine secondary antibody. Finally, VECTASHIELD® Antifade Mounting Medium was used to mount the cells and FFPE sections.

The Leica TCS SP5 Confocal Spectral Microscopy Imaging System (Leica, Wetzlar, Germany) acquired fluorescence images. The photobleaching FRET method was established according to the manufacturer's instructions (FRET Wizards in the Leica Application Suite) and described in our previous paper [21]. The following formula was used to estimate FRET efficiency: $FRET_{eff} = (D_{post}\text{-}D_{pre})/D_{post}$. We calculated the FRET efficiency of at least 15 cells for analysis.

2.7. Animals

NOD-SCID-IL2Rγ^{null} (NSG) mice were purchased from BioLASCO Taiwan Co., Ltd (Taipei, Taiwan)

and were raised following an Association for the Assessment and Accreditation of Laboratory Animal Care-approved protocol (LAC-101-0064).

Cell-derived xenograft (CDX) model was used cell (231-WT, 231-Vc, 231-SIK3, 231-Cas9 C, and 231-SIK3 KO)-derived xenograft tumors. The tumor was divided into four equal tissue blocks ($3 \times 3 \times 3$ mm^3, n = 4 per stable cell). A puncture needle was used to implant the tumor blocks on the fat pad between the third and fourth mammary glands in NSG mice. The tumor growth was measured with a caliper every two days. Tumor size = Length × Width^2/2.

PDX model was used SIK3 high-expressing PDX tumors were purchased from Jackson Lab Co. USA (form J000111056) and were divided into approximately 8 equal blocks ($3 \times 3 \times 3$ mm^3). A puncture needle was used to implant the tumor blocks on the fat pad between the third and fourth mammary glands in NSG mice (n = 8). The tumor size was observed and measured for four weeks, and curcumin treatment (40 mg/kg, dissolved in corn oil, n = 4) was started at the fifth week after transplantation. Tumor growth was observed and measured for 12 days, three times a week. The tumor growth size was measured with a caliper. Tumor size = Length × Width^2/2.

2.8. Statistical analysis

All data are presented as the mean ± SEM of more than three independent experimental replicates. *SIK3* mRNA expression levels in paired normal adjacent and tumor tissues from breast cancer patients were compared using a two-tailed Mann–Whitney U test. One-way ANOVA was used to calculate the pathological and grade data statistically. The two-tailed t-test was used to analyze other groups. SigmaPlot plotting software and Social Science Statistical Software Package (SPSS) v.11.0.0 was used for all statistical comparisons. A *p*-value of 0.05 or less indicated statistical significance.

3. Results

3.1. High SIK3 expression was detected in human breast cancer tissues and cells

A previous study showed that SIK3 expression was detected in approximately 55% of breast cancer patients [18]. qPCR verified this observation. The results show that higher levels of *SIK3* mRNA were detected in human breast tumor tissue samples (n = 342) (Fig. 1a). In addition, the absolute copy number of *SIK3* mRNA expression in tumor (T) tissue is higher than that in normal (N) adjacent tissues (Fig. 1b). Correspondingly, the statistical data is subdivided into two groups (i.e., tumors are higher than normal neighbors, T > N vs. normal neighbors are higher than tumors, N > T). The expression of *SIK3* mRNA in tumor tissues of the T > N group was significantly higher than that of normal adjacent tissues (Fig. 1c). In order to explore the clinical standard demographic assessment and the fold change of *SIK3* mRNA expression between normal adjacent and tumor paired samples, the results are shown in Table 1. Higher *SIK3* mRNA expression is positively correlated with high-grade breast cancer (Fig. 1d and Table 1). In addition, SIK3 protein levels in breast tumor tissues were detected by IHC staining. The results show that the expression level of SIK3 protein in tumor cells was higher (Fig. 1e, red box). The expression level of SIK3 protein in breast cell lines was further observed. The results show that higher SIK3 was detected in most breast cancer cells, especially in MDA-MB-453, T47D, and MDA-MB-231 cells (Fig. 1f). The above results proved that higher levels of SIK3 protein were detected in breast cancer tissues and cell lines.

3.2. Overexpression of SIK3 in tumor cells promotes cell growth and migration

SIK3 has been reported as an immunogenic target for ovarian cancer and has a tumorigenic effect that promotes cancer progression [18]. To explore whether SIK3 is involved in promoting breast cancer tumors, two stable cells overexpressing SIK3 (derived from SKBR3, named SK-SIK3 and MDA-MB-231, called 231-SIK3) and two stable cells depleting SIK3 (derived from MDA-MB-231, named 231-Si or 231-SIK3-KO) were established by siRNA and gene knockout, respectively. Their SIK3 expression levels were confirmed by Western blotting (Fig. 2a). The results of cell growth curve measurement indicate that SIK3 is a positive regulator of cancer cell growth. The experimental results showed that SK-SIK3 and 231-SIK3 grew faster than the control cells (SK-Vc and 231-Vc) (Fig. 2b, red triangle). In contrast, cell growth was inhibited in SIK3-depleting stable cells (231-Si and 231-SIK3 KO cells) (Fig. 2b, green square). Colony-forming experiments demonstrated that 231-SIK3 cells grew faster and formed larger colonies than control cells (Fig. 2c, red bars). In contrast, 231-Si and 231-SIK3 KO cells grew more slowly and formed small colonies than control cells (Fig. 2c, green bars).

Furthermore, the correlation between the SIK3 expression status and migration was explored by wound-healing and Transwell assays. The results showed that overexpression of SIK3 promoted migration (Fig. 2d, red bars), while SIK3 inhibition reduced the migration activity of MDA-MB-231 cells (Fig. 2d, green bars).

3.3. SIK3 promotes cancer cell migration by upregulating the expression of mesenchymal (M) markers

In order to explore the molecular mechanism of SIK3 involved in tumor cell migration, the expression of epithelial–mesenchymal transition (EMT)

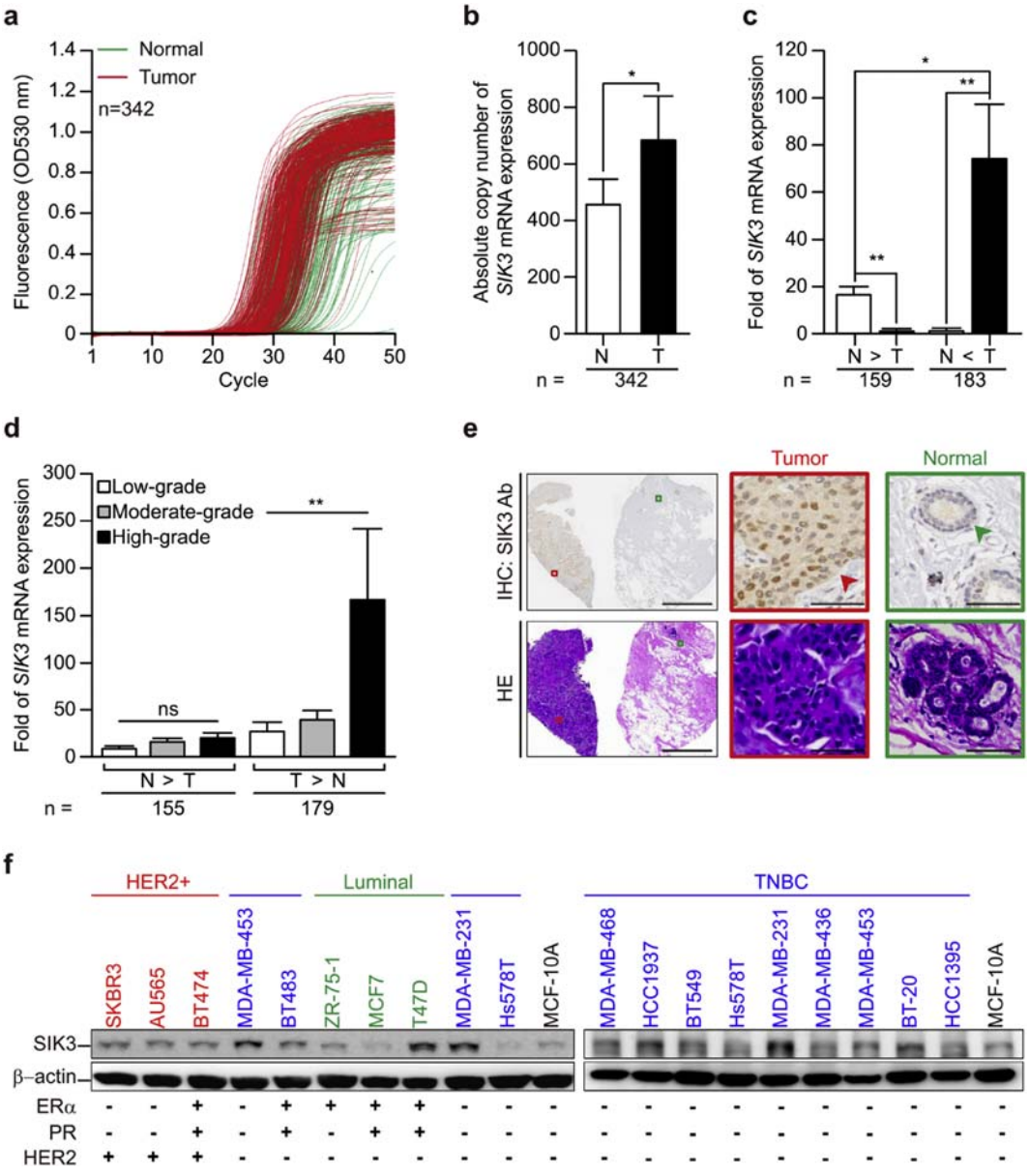

Fig. 1. ***SIIK3 overexpression was detected in breast cancer tumor cells.*** *(a and b) Amplification curves of qPCR (tumor, red lines vs. normal adjacent, green lines) (a), and quantitative comparison of SIK3 mRNA expression by absolute copy numbers. (b), in paired human breast tumors and normal adjacent tissues (n = 342) were detected by qPCR. (c and d) The quantitative comparison of SIK3 mRNA expression was subdivided into two groups according to the fold increasing in the N > T and T > N groups. (c) and clinical-grade status (d). (e) Representative IHC staining of SIK3 and HE images in breast cancer and normal adjacent tissues. Scale bars = 2 mm (left) and 50 μm (right, red, and green box images). (f) Subdivide breast cancer cell lines into three groups (HER2+, TNBC, and Luminal) based on ER/PR/HER2 status. Normal breast epithelial cell (MCF-10A) was used as normal control. Western blot results showed the expression levels of SIK3 protein, and β-actin was used as a protein loading control. The data are the mean ± SEM value. A two-tailed Mann–Whitney U test (b and c) and One-way ANOVA (d) test were used to calculate the p-values. *p < 0.05, **p < 0.01, and ns = no significant.*

markers was analyzed by Western blotting (Fig. 2e). Malignant cells acquire M-markers (such as Vimentin, β-catenin, N-Cadherin, αSMA, Snail, Fibronectin, Vitronectin, and MMPs) and lost epithelial (E)-markers (such as E-Cadherin, Mucin-1, Cytokeratin, Occludin, and Desmoplakin) in the EMT process [22,23]. M-markers are highly expressed in SIK3 overexpression (231-SIK3) cells (Fig. 2e, bottom, right panels). In contrast, the expression of M-markers decreased in 231-Si cells, while the epithelial markers increased (Fig. 2e, bottom, left panel). RNA sequencing analysis was further used to explore the differences in gene expression profiles in 231-Vc and 231-SIK3 cells (Fig. 2f, middle panel). It was observed that *SIK3* expression was consistently correlated with EMT markers. The heatmap shows that 231-SIK3 cells have a mesenchymal phenotype (i.e., higher expression of M-markers) (Fig. 2f, middle panel). Gene Set Enrichment Analysis (GSEA) analysis showed that SIK3 overexpression significantly enriched the EMT gene (Fig. 2f, right panel). GSEA results show that SIK3 overexpressing cells have a mesenchymal phenotype and high metastatic potential.

3.4. SIK3 promotes tumor growth and cell cycle progression

In order to clarify the role of SIK3 in cell growth cycle progression, we analyzed SK-Vc and SK-SIK3 cells by flow cytometry to evaluate the correlation between SIK3 protein levels and cell growth cycle progression in a time-dependent manner (Fig. 3a, n = 2). Cells were cultured in 0.04% FBS for 48 h for synchronization [24]. After reactivating the cells

Table 1. Clinical parameters and fold differences in SIK3 mRNA expression in paired tumor/normal adjacent samples.

Parameter	T > N group (#)			N > T group (#)		
	n =	Mean (§) ± S.E.	P	n =	Mean (§) ± S.E.	P
Age			0.23			0.31
≤ 50 y	69	43.10 ± 15.40		52	13.1 ± 2.10	
> 50 y	102	103.40 ± 39.80		106	18.5 ± 3.50	
Pathology			0.99			0.92
Ductal Carcinoma in Situ	7	32.0 ± 28.00		5	6.8 ± 2.30	
Invasive Ductal Carcinoma	160	77.5 ± 25.80		141	17.4 ± 2.80	
Invasive Lobular Carcinoma	5	27.1 ± 24.10		6	6.9 ± 2.50	
Mucinous Carcinoma	3	3.5 ± 1.90		4	17.7 ± 11.40	
ER			0.53			0.28
Negative	41	48.2 ± 25.80		40	12.0 ± 3.50	
Positive	140	83.2 ± 29.10		119	18.2 ± 3.10	
PR			0.44			0.14
Negative	63	50.8 ± 18.50		75	12.8 ± 2.30	
Positive	117	89.0 ± 34.50		84	20.1 ± 4.20	
HER2			0.46			0.33
Negative	144	84.8 ± 29.00		124	18.1 ± 3.00	
Positive	34	40.0 ± 14.90		31	12.0 ± 3.30	
TNBC			0.70			0.85
No	161	75.1 ± 25.40		137	16.8 ± 2.70	
Yes	21	73.1 ± 48.50		22	15.5 ± 6.10	
Stage			0.94			0.18
1 & 2	88	60.3 ± 22.60		82	18.5 ± 3.30	
3 & 4	44	52.7 ± 18.12		23	9.92 ± 2.20	
Grade			0.04			0.41
Low	28	27.2 ± 10.20		17	8.8 ± 3.00	
Moderate	97	39.6 + 9.70		84	16.2 ± 2.90	
High	54	166.9 ± 74.80		54	20.3 ± 5.60	
Recurrence			0.88			0.55
No	59	36.8 ± 10.30		35	9.6 ± 1.60	
Yes	9	29.9 ± 26.30		7	12.6 ± 8.10	
Survival			0.13			0.55
Alive	61	35.7 ± 10.00		39	9.5 ± 1.70	
Dead	8	32.9 ± 29.60		4	16.8 ± 11.20	

#: Data were obtained for 342 breast cancer patients and divided into N > T and T > N groups. §: Average fold differences in *SIK3* mRNA expression in each group. The data were the mean ± SEM values. One-way ANOVA was used to analyze the pathological and grade data; other data were analyzed with a two-tailed Mann–Whitney U test.

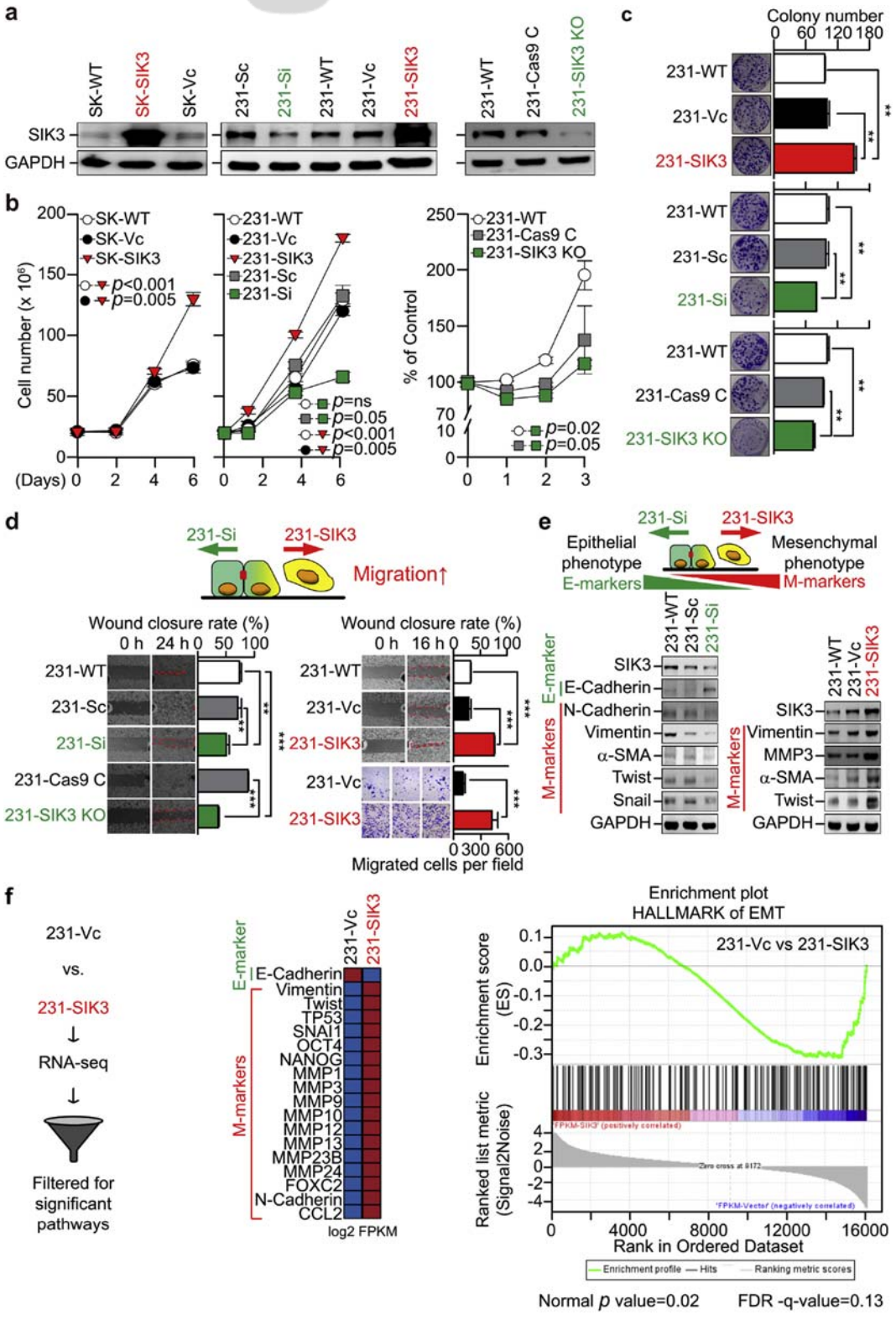

Fig. 2. ***SIK3 overexpression promotes TNBC cell growth and migration.*** *(a) Western blot results displayed SIK3 and GAPDH in WT (SKBR3 and MDA-MB-231) and stable cells (SK-Vc, SK-SIK3, 231-Vc, 231-SIK3, 231-Sc, 231-Si, 231-Cas9 C, and 231-SIK KO). GAPDH was used as a protein loading control. (b–d) Proliferation (b), colony formation (c), and migration (d) assays were used to assess the tumorigenicity of SIK3 expressing stable cells. The data are the mean ± SEM values. The two-tailed t-test was used to calculate the p-values. **p < 0.01, ***p < 0.001. Scale bars = 250 μm (d). (e) SIK-induced EMT markers changed in MDA-MB-231 cells. Western blot was performed, and the GAPDH was used as a protein loading control. (f) Schematic illustration of RNA-seq analysis flow chart of 231-Vc and 231-SIK3 stable cells (left). The heatmap*

with 10% FBS, SK-SIK3 cells re-entered the G0/G1 and S phase cell cycle faster than SK-Vc cells (control cells). The percentage of SK-SIK3 cells in G0/G1 and S phases decreased, respectively (i.e., 6 h, green arrow and 12 h, blue arrow). Meanwhile, the percentage of the G2/M phase increased at 6 h and 12 h (red arrows). The levels of G1/S cell cycle regulatory proteins level were determined by Western blot. The results show that SIK3 overexpression increased the expression of cyclin D, the phosphorylation of retinoblastoma protein (p-Rb), and E2F proteins, while the CDK inhibitor p27 was down-regulated (Fig. 3b). In summary, the overexpression of SIK3 in cancer cells promotes the transition of the G1/S phase and promotes the cell cycle.

3.5. SIK3 affects cell growth through the interaction of cyclin D and p27 protein

The activation of CDK4/cyclin D complex is a crucial process of Rb hyperphosphorylation, triggering the G1/S phase transition of the cell cycle [9]. A photobleaching FRET assay was used to test whether SIK3 affects the cell growth cycle by interacting with cell cycle regulatory proteins (CDK4/cyclin D complex and p27) (Fig. 3c). It was observed that SIK3 overexpressing (SK−SIK3 and 231-SIK3) cells detected significant FRET activity between SIK3 and cyclin D but not CDK4 (Fig. 3c, white arrow). In order to test whether SIK3 interacts with p27 (a negative regulator of CDK4 assembly), the FRET activity of the cell was examined. It was found that the FRET activity between SIK3 and p27 was lower than that of cyclin D in cells overexpressing SIK3 (SK−SIK3 and 231-SIK3) (Fig. 3c, yellow arrow). These results imply that the subcellular localization and protein−protein interaction of SIK3 and cell cycle inhibitor protein p27 determine their potential cancer treatment functions and prognosis. We further performed photobleaching FRET assays in tissue microarrays to verify the interaction of SIK3 and p27 in tumors and adjacent normal tissues (Fig. 3d, n = 110). The results show that the p27/SIK3 interaction was significantly detected in tumor slices (fold = 25.16, n = 100; red box, yellow arrows) compared to normal slices (fold = 2.65, n = 10; green box) (Fig. 3d). These results indicated that SIK3 participates in tumor growth through the interaction of cyclin D and p27 complex.

This hypothesis was confirmed by using a CDX model to test the tumor growth-promoting effect of SIK3 *in vivo*. We transplanted TNBC tumor cells with various SIK3 expression states (MDA-MB-231, 231-SIK3, SIK3−KO, and vector control cells) into immunodeficiency (NSG) mice to evaluate tumor growth curves (Fig. 4a and b). The results showed that the increase in SIK3 protein expression significantly promoted tumor growth in 231-SIK3 xenograft mice (Fig. 4a, n = 4). In contrast, inhibiting SIK3 expression in 231-SIK3 KO cells inhibited tumor growth in CDX mice (Fig. 4b).

3.6. Curcumin inhibits SIK3-mediated TNBC tumor growth promotion in vivo

The above results indicate that SIK3 is a prominent molecular target and has valuable potential in finding beneficial natural compounds to target SIK3 expression levels in TNBC cancer cells (Fig. 4c). Western blot results show that curcumin is the most effective in inhibiting SIK3 expression in MDA-MB-231 cells (Fig. 4c, left panel). In addition, the expression of SIK3 in MDA-MB-231 cells was detected by Western blotting after curcumin treatment in a dose-dependent manner (0−50 μM, 24 h) (Fig. 4c, right panel). Furthermore, Western blot results showed that the expressions of SIK3, cyclin D, and CDK4 were down-regulated after curcumin treatment in a dose-dependent manner. Conversely, the expression of p27 is upregulated (Fig. 4c, right panel). These results indicate that curcumin is a potential therapeutic agent for inhibiting SIK3-mediated tumor cell growth. We further tested the anti-migration effect induced by curcumin in SIK3 overexpressing TNBC cells through wound healing tests, and the results showed that curcumin significantly inhibited SIK3-induced TNBC cell migration (Fig. 4d).

The results described in Fig. 1f indicate that SIK3 protein is preferentially detected in TNBC tumor cells. The commonly used hormonal and targeted therapy is not adequate for TNBC after surgery. Chemotherapy is the only option for postoperative adjuvant treatment for TNBC patients. The current trend is to give the received chemotherapy course before surgery (i.e., pre-surgical chemotherapy) to shrink the tumor then undergo surgery. Dietary nutrients (such as curcumin) should help TNBC patients undergoing chemotherapy. To test this

(red = upregulated, blue = down-regulated) of RNA-Seq transcriptome analysis showed the expression of metastasis-related genes in 231-Vc and 231-SIK3 cells (middle). Gene Set Enrichment Analysis (GSEA) plots of RNA-seq data revealed EMT gene signatures in 231-Vc and 231-SIK3 cells (right). An empirical gene-based permutation test determined the nominal p-values. The green line indicated enrichment profile, the black vertical lines indicated the hit, and the gray vertical line indicated the ranking index score.

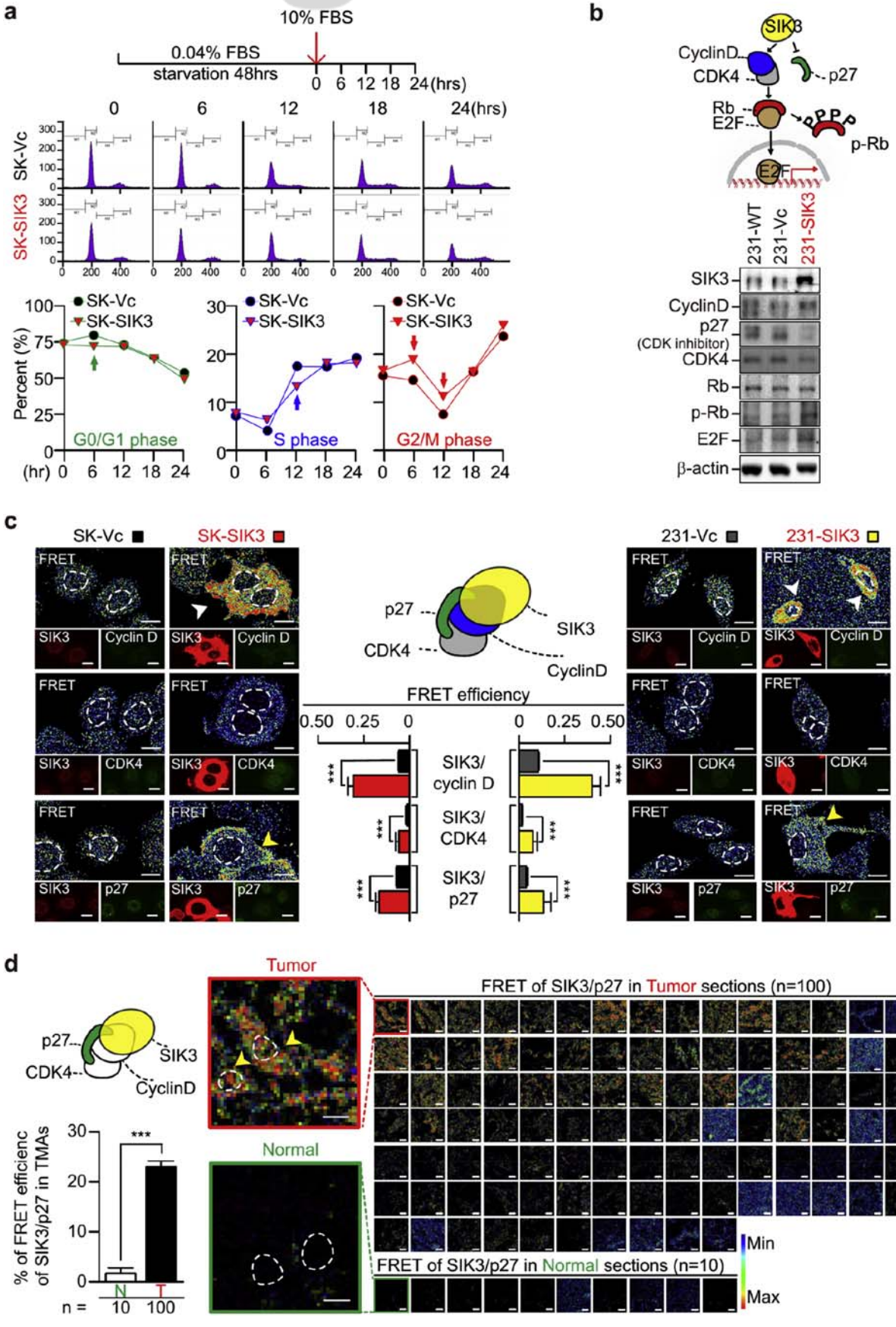
a
10% FBS
0.04% FBS
starvation 48hrs
0 6 12 18 24(hrs)
SK-Vc
SK-SIK3
Percent (%)
G0/G1 phase
S phase
G2/M phase
b
SIK3
CyclinD
CDK4
p27
Rb
E2F
p-Rb
231-WT
231-Vc
231-SIK3
β-actin
c
SK-Vc
SK-SIK3
231-Vc
231-SIK3
FRET
SIK3
Cyclin D
CDK4
p27
FRET efficiency
SIK3/ cyclin D
SIK3/ CDK4
SIK3/ p27
d
Tumor
Normal
FRET of SIK3/p27 in Tumor sections (n=100)
FRET of SIK3/p27 in Normal sections (n=10)
Min
Max
% of FRET efficienc of SIK3/p27 in TMAs
n = 10 100

hypothesis, we established patient-derived tumor xenograft mice from TNBC patients (TNBC-PDX) to test the anticancer effect of curcumin (40 mg/kg, three times a week, IP injection, n = 4) (Fig. 4e). The results show that curcumin treatment significantly reduced tumor growth volume (Fig. 4e). We further performed Western blot analysis to confirm the molecular mechanism of curcumin and determine protein levels. In curcumin-treated TNBC-PDX tumors, proto-oncoproteins (N-cadherin, Snail, and cyclin D) were down-regulated, and CDK inhibitors (p27) were upregulated. Interestingly, curcumin treatment did not affect the expression of E-Cadherin (Fig. 4f). We further evaluated the expression of proteins involved in cell proliferation and apoptosis in PDX tumor tissue by IHC (Fig. 4g, bottom, left panel) and TUNEL staining (Fig. 4g bottom, right panel). The results showed that in curcumin-treated TNBC-PDX tumors, Ki67 cell proliferation markers were decreased, and apoptotic cells increased, which had an anti-proliferative effect (Fig. 4g).

In summary (Fig. 4h), this study confirmed that SIK3 overexpression accelerates the growth of cancer cells by activating cyclin D and inhibiting the expression of p27 in TNBC cells. Our findings confirm that SIK3 can be used as a molecular target for TNBC tumor therapy. From the perspective of chemoprevention, curcumin has excellent clinical application value.

4. Discussion

Chemotherapy is the main treatment option for TNBC. However, TNBC patients are often found to be resistant to chemotherapy [2]. Several studies had shown that curcumin combined with chemotherapy could enhance the synergistic antitumor effect, thereby obtaining better therapeutic effects and reducing the side effects of chemotherapy [25,26]. Recent clinical trial studies have provided clinicians with the necessary information to design new and improved robust therapeutic interventions. The NCT03072992 report showed that breast cancer patients who received curcumin (300 mg solution) and paclitaxel (80 mg/m^2) had a significantly higher overall response rate (ORR) than patients who received placebo [7]. The NCT01490996 report showed that curcumin (2 g) combined with FOLFOX-based chemotherapy showed a higher ORR (53.3%) in patients with metastatic colorectal cancer than those receiving FOLFOX-based monotherapy (11.1%) [26]. These clinical trials lead us to believe that curcumin is beneficial for developing new breast cancer treatment strategies with different combinations. Due to its pleiotropic biological activity, curcumin has excellent potential in anticancer treatment. However, its poor solubility and bioavailability may limit its clinical application. A new curcumin formula was designed to overcome these shortcomings, such as bio-based nanoparticles [27] and metal-curcumin complexes [28]. These new formulas increase solubility, cell absorption, and bioavailability and enhance curcumin's antioxidant, anti-inflammatory, antibacterial, and antiviral effects.

In this study, the TNBC-PDX model was used to observe the antitumor effect of curcumin. PDX tumors are derived from tumors of TNBC patients after surgery. Breast cancer is a heterogeneous disease. Different patients will have a different impact after receiving the same treatment. Even if patients receive the same treatment at other times, different effects will be produced. This heterogeneous feature makes breast cancer difficult to cure, especially for TNBC patients. PDX tumors have a similar microenvironment with patients, but CDX tumors do not. Therefore, PDX tumors can simulate small-scale clinical trials in breast cancer patients. PDX is also easier to find the best treatment strategy and dosage. In this study, the TNBC-PDX model was used to verify the antitumor efficacy of curcumin. The results showed that curcumin could effectively inhibit the growth of TNBC-PDX tumors (Fig. 4e). Curcumin has the same antitumor efficacy in other PDX tumor models [29].

In addition, we verified the expression levels of SIK1, SIK2, and SIK3 in breast cancer cell lines in the CellExpress database (http://cellexpress.cgm.ntu.edu.tw/). The results showed that SIK1 could not be detected in breast cancer cell lines, while SIK1 and SIK2 were highly expressed in breast cancer cell lines. Previous studies had shown that

Fig. 3. ***SIK3 promotes cell cycle progression through the interaction of cyclin D and p27 protein.*** *(a) Schematic representation of the research design (Top). Flow-cytometric analysis was used to analyze the cell cycle distribution of SK-Vc and SK-SIK3 cells (middle). The quantitative comparison results were shown at the bottom (n = 2). (b) Schematic illustration of SIK3 and G1/S transition (Top). Western blot results showed the expression levels of SIK3, β-actin, and G1/S transition-related proteins in SK-Vc and SK-SIK3 stable cells. β-actin was determined as a protein loading control. (c) In SKBR3 (left) and MDA-MB-231 (right), the interaction of SIK3 and cell cycle regulatory proteins (cyclin D, CDK4, and p27) was detected by FRET analysis. The quantitative analysis results are presented (middle). (d) FRET images detected the SIK3/p27 interaction, and the quantitative results in the breast cancer tissue microarray (n = 110) were displayed. Scale bars = 10 μm (c and d). The data are the mean ± SEM values. The two-tailed t-test was used to calculate the p-values. ***p < 0.001.*

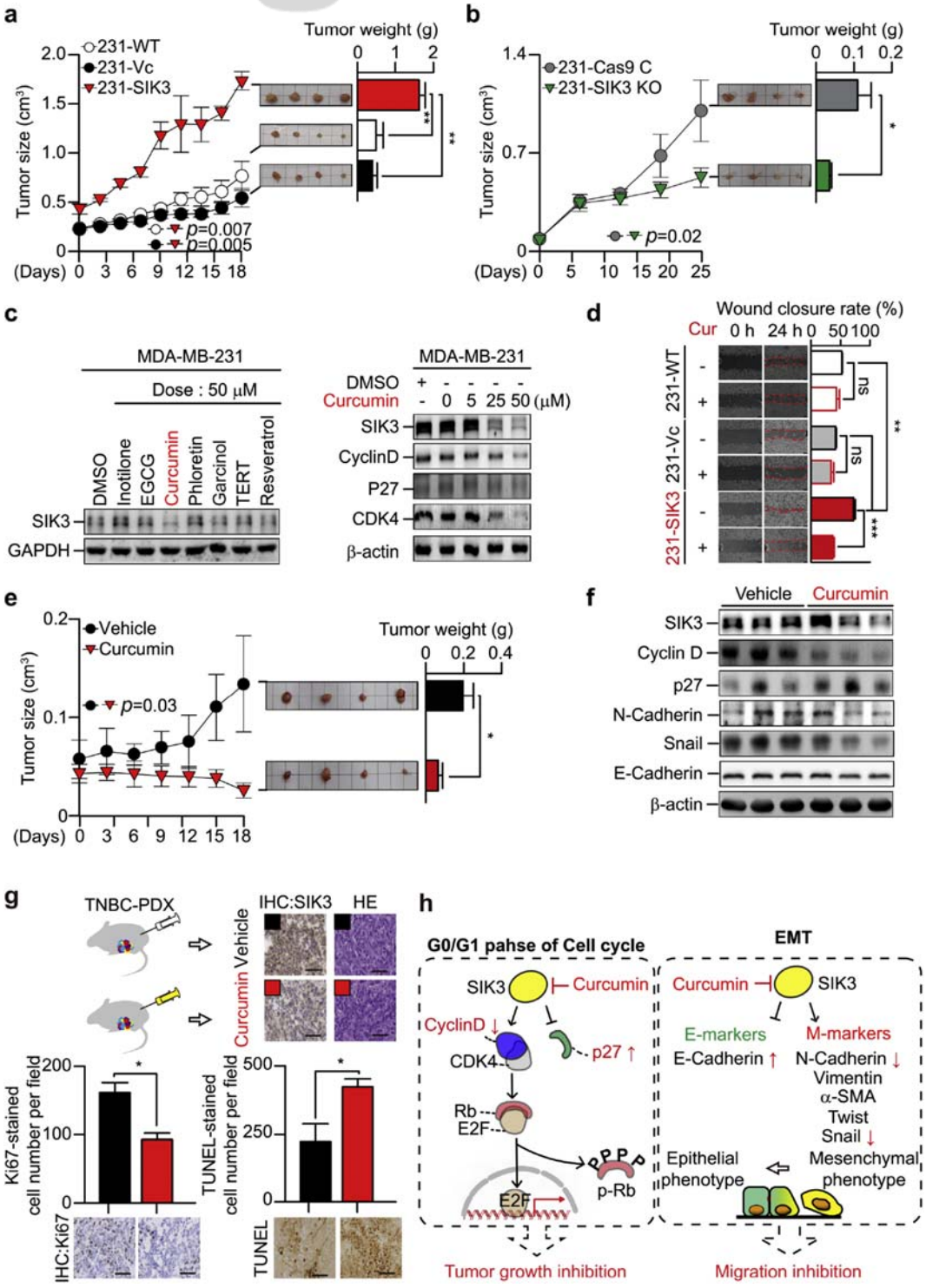

Fig. 4. ***Curcumin inhibits SIK3-mediated TNBC tumor growth promotion in vivo.*** *(a and b) The 231-SIK3 and 231-SIK3 KO cells were transplanted into NSG mice (n = 4), and the tumor growth curve was measured. Compared with the control (231-Wt, 231-Vc, and 231-Cas9 C), the tumor growth curve and excised tumor weights with overexpression (231-SIK3) (a) and SIK3 depletion (231-SIK3 KO) (b) changed significantly. (c) MDA-MB-231 cells were treated with natural compounds (50 μM) for 24 h. Western blot results showed the protein level of SIK3 (left). GAPDH was tested as a protein loading control. MDA-MB-231 cells were treated with curcumin in a dose-dependent manner (0–50 μM) for 24 h (right). Western blot results displayed the protein levels of SIK3 and cell cycle regulatory proteins. β-actin expression was detected as a protein loading control. (d) SIK3 expressing MDA-MB-231 stable (231-SIK3) cells were treated with curcumin (25 μM, 24 h) for wound healing tests. 231-WT and 231-Vc cells were treated with the same protocol as the control. Scale bars = 250 μm. (e) Curcumin (40 mg/kg, 3 times a week, IP injection, n = 4) was used to treat TNBC-PDX tumor mice, and the tumor growth curve was determined. (f) At the end of the sacrifice, the protein was harvested from TNBC-PDX tumor*

SIK3 was used as a tumor marker antigen for diagnosing ovarian cancer, but the detailed molecular mechanism was not elucidated [30]. This study clarified the molecular mechanism of SIK3-mediated tumor growth for the first time. The results showed that SIK3 upregulated the expression of cyclin D and down-regulated the expression of p27, which in turn triggers the phosphorylation of Rb and E2F release, thereby promoting the transition of G1/S and accelerating the cell cycle process (Fig. 3a and b). It had been reported that curcumin inhibited cell proliferation by down-regulation of cyclin D1 expression and CDK4-mediated phosphorylation of Rb protein [30]. The tumor microenvironment contains a variety of immune cells, such as tumor-associated macrophages (TAMs), to mediate the progression and proliferation of cancer. TAM is the main cell source of IL-17 in breast tumors. IL-17 directly promotes breast cancer cell invasion *in vitro* [31]. A previous study showed that high salt and IL-17 synergistically induced SIK3-mediated cancer cell proliferation and MMP-9-activated tumor metastatic CXCR4 expression [16]. Our results show that SIK3 upregulates the expression of M-markers (such as Vimentin, α-SMA, Twist, and MMP-3) and down-regulates the expression of E-markers (Fig. 2e and f), thereby promoting cell migration (Fig. 2c). Next, curcumin treatment inhibited SIK3-mediated migration in SIK3 overexpressing cells (Fig. 4d). Therefore, SIK3 may serve as an attractive target with potential prognostic or therapeutic value in IL-17-mediated invasion.

p27 is an atypical tumor suppressor, and overexpression of p-p27 has been detected in a variety of cancers [32]. Cytoplasmic p27 promotes cell proliferation and migration [11]. It was observed that p27 was seen in the cytoplasm and nucleus, and the intense FRET activity of the SIK3/p27 complex was detected in the cytoplasm of SIK3 overexpressing cells (Fig. 3c). The SIK3/p27 complex has intense FRET activity in breast cancer tissue microarrays (Fig. 3d). In addition, Guiley et al. used the structural analysis of the active complex of CDK4 with cyclin D1 and p27 to confirm that the phosphorylation of $p27^{Y74}$ reshaped the active site of CDK4, making it fully activated. In addition, the active $phosp27^{Y74}$-CDK4-Cyclin D1 trimer loses its affinity with the CDK4 inhibitor palbociclib [33]. The above results indicated that the complex formation of p27 and SIK3 effectively inhibited the antitumor activity of p27 in TNBC tumor cells. Therefore, detecting the phosphorylation status and cellular localization of p27 is essential for future exploration of the interaction between p-p27 and SIK3 protein in TNBC carcinogenesis. Thus, the SIK3/p27 complex can be used as a biomarker for the treatment or prognosis of TNBC.

In summary, by identifying SIK3's promotion of cell cycle progression and migration and its contribution to clinical outcomes, it provides a framework for testing new curcumin-targeted SIK3 treatments in TNBC. Further efforts are needed to clarify the interaction between SIK3 and p27 and explore the effect of p27 phosphorylation status on breast cancer. It is expected that SIK3 will serve as a targeted marker and lead to its clinical transformation.

Author contributions

Yun Yen, Shih-Hsin Tu, Li-Ching Chen, and Yuan-Soon Ho conceptualized and designed the experiments. Shih-Hsin Tu, Li-Ching Chen, and Yuan-Soon Ho acquired funding. Tzu-Chun Cheng, John Oliver Sayseng, Ting-Ching Juan, Chia-Lang Fang, You-Cheng Liao, Cheng-Ying Chu, and Hui-Wen Chang conducted experimental works and data analyses. Shih-Hsin Tu provided human breast cancer samples. Tzu-Chun Cheng, Li-Ching Chen, and Yuan-Soon Ho wrote the manuscript and compiled it with contributions from the other authors. All authors reviewed the manuscript.

Conflicts of interest

The authors declare that this study had no competing financial interests or financial relationships with other people or organizations.

*tissue. Western blot was performed to determine the protein levels of SIK3, N-Cadherin, Snail, E-cadherin, cyclin D, and p27. The protein expression of β-actin was used as a protein loading control. (g) Tumor sections were obtained from TNBC-PDX mice exposed to curcumin as described above. (g) Representative IHC staining of SIK3 and HE images were shown on tumor sections of TNBC-PDX mice (n = 4) (Top). Ki67 was used as a proliferation marker. The TUNEL assay identified apoptotic cells. Representative IHC staining and the quantification of the Ki67+ and TUNEL + cells were shown on the bottom (left: Ki67+ cells, right: TUNEL + cells). (h) The diagram illustrates the molecular mechanism by which SIK3 promotes cell cycle progression and migration. Left: SIK3 promotes the cell cycle process by upregulating the expression of cyclin D, down-regulating the expression of p27, and hyperphosphorylation of Rb protein, thereby triggering the G1/S transition. Right: SIK3 promotes the expression of M-markers (such as Vimentin, N-Cadherin, αSMA, Snail, and MMPs) and inhibits the expression of E-markers (E-Cadherin), resulting in enhanced migration ability. In TNBC tumor cells exposed to curcumin, SIK3-mediated cell growth cycle and EMT mechanisms are inhibited. All data are the mean ± SEM values. A two-tailed t-test was used to calculate the p-values. *p < 0.05, **p < 0.01, ***p < 0.001, and ns = no significant. Scale bars = 250 μm (d) and 50 μm (g).*

Acknowledgments

This study was supported by the Health and Welfare Surcharge of Tobacco Products grant (MOHW110-TDU-B-212-144014); Ministry of Science and Technology, Taiwan.

MOST108-2320-B-038-033-MY3 and 110-2320-B-038-082 awarded to Yuan-Soon Ho, MOST109-2314-B-038-033-MY3 awarded to Shih-Hsin Tu, and MOST109-2320-B-038-017 and 110-2320-B-038-031 awarded to Li-Ching Chen as well as "TMU Research Center of Cancer Translational Medicine" from The Featured Areas Research Center Program within the framework of the Higher Education Sprout Project by the Ministry of Education (MOE) in Taiwan. We thank TMU's CRISPR gene targeting core laboratory for technical assistance.

Appendix.

Supplementary materials and methods

Chemicals and antibodies

G418 disulfate salt (catalog #4131) was purchased from Bio-Techne (Minneapolis, MN, USA).

The following commercial antibodies (catalog number and manufacturer) were used for immunofluorescence (IF) staining, western blotting, and IHC staining according to the manufacturers' instructions: anti-SIK3 (HPA048161, Sigma−Aldrich, USA), anti-MMP3 (GTX 100724, GeneTex, Irvine, CA, USA), anti-GAPDH (GTX627408, GeneTex, Irvine, CA, USA), anti-Ki67 (GTX16667, GeneTex, Irvine, CA, USA), anti-Vimentin (#5741, Cell Signaling Technology, Beverly, MA, USA), anti-Snail (#C15D3, Cell Signaling Technology, Beverly, MA, USA), N-Cadherin (#7074, Cell Signaling Technology, Beverly, MA, USA), anti-p-RB (Sc-377528, Santa Cruz Biotechnology, CA, USA), anti-RB (GTX100545, GeneTex, rvine, CA, USA), α-SMA (A2547, Sigma−Aldrich, St. Louis, MO, USA), anti-Twist (AB50887, Abcam, Cambridge, UK), anti-E-Cadherin (#610182, BD Transduction Laboratories, Lexington, KY, USA).

Construction of plasmids

For SIK3 overexpression plasmid: PCR was used to amplify the selected SIK3 sequences. The PCR conditions were as follows: 94 °C for 3 min; 94 °C for 30 s, 60 °C for 20 s, and 72 °C for 90 s for 35 cycles of amplification; finally, 72 °C for 7 min. The SIK3 specific fragment was inserted into the pcDNA3.1 expression vector (V790-20, Thermo Fisher Scientific, Waltham, MA, USA) cut by *Bam*H1 and *Xho*I to generate the pcDNA3.1-SIK3 overexpression vector. The primers used in this study were as follows: SIK3 specific forward 5′-AATGGATCCGCCAC-CATGGCGGCGGCGGCGGCGAG, and SIK3 reverse 5′-AATCTCGAGTTACACGCCTGCCTGCTCCA.

For SIK3 sc/siRNA plasmid: Use Oligoengine 2.0 to predict and design a sequence for effective RNA interference to SIK3. The specific forward fragments −SIK3 scramble forward 5′-GATCCCCACG-TACGTGTCCACACACTTTCAAGA-GAAGTGTGTGGACACGTACG TTTTTTA, SIK3 scramble reverse 5′-AGCTTAAAAAACG-TACGTGTCCACACACTTCTC TTGAAAGTGTGTGGACACGTACGTGGG, SIK3 siRNA forward 5′-GATCCCCCAACC ATCTCTT-CAGGCAGTTCAAGAGACTGCCTGAAGA-GATGGTTGTTTTTA, and SIK3 siRNA reverse 5′-AGCTTAAAAA-CAACCATCTCTTCAGGCAGTCTCTT-GAACTGCCT GAAGAGATGGTTGGGG were inserted into *Bgl*II- and *Hind*III-cut pSUPER.retro.neo-GFP plasmids (Oligoengine, Seattle, WA, USA) to generate pSUPER-SIK3 scRNA and pSUPER-SIK3 siRNA.

For SIK3 knockout plasmid:sgRNA is designed with the CHOPCHOP online tool (https://chopchop.cbu.uib.no/), insert the sgRNA coding sequence into the pAll-Cas9-pPpuro plasmid from National RNAi Core Facility (Academia Sinica, Taipei, Taiwan). The sequence of sgRNA targeting the human SIK3 gene (NM_025164.6) is as follows: sgRNA is 5′-TGGCA GAAAAGGAGGCACGTCGG-3'.

Generation of stable cells

For SIK3-overexpressing stable cells: SKBR3 and MDA-MB-231 cells were transfected with 2 μg of plasmids (pcDNA3.1 and pcDNA3.1-SIK3 plasmids) using the Neon Transfection System (Thermo Fisher Scientific, Waltham, MA, USA). The transfected cells were selected with G418 (200 μg/mL or 6 mg/mL). After 30 days of selection, stable cells (SK-Vc, SK-SIK3, 231-Vc, and 231-SIK3) were established.

For SIK3-depleted stable cells: MDA-MB-231 cells were transfected with 2 μg of plasmids (pSUPER-SIK3 scRNA and pSUPER-SIK3 siRNA) using the Neon Transfection System (Thermo Fisher Scientific, Waltham, MA, USA). The transfected cells were selected with G418 (6 mg/mL). After 30 days of selection, stable cells (231-Sc and 231-Si) were established.

For SIK3 knockout (KO) stable cells: The sgRNA plasmid was transfected into MDA-MB-231 cells by Neon Transfection System (Thermo Fisher

Scientific, Waltham, MA, USA). The transfected cells were screened with 2 μg/mL puromycin for 1 week. SIK3 KO cells (named 231-SIK3 KO) were limited to 96-well plates and isolate single-cell clones. The Neon transfection system (Thermo Fisher Scientific, USA) was used to transfect the pAll-Cas9-pPpuro plasmid into MDA-MB-231 cells, and the transfected cells were named 231-Cas9 C. The generation of 231-Cas9 C cells was performed according to the same protocol as 231-SIK3 KO cells. 231-SIK3 KO cells were confirmed by DNA sequencing of genomic regions. Finally, Western blot analysis confirmed the expression levels of 231-Cas9 C and 231-SIK3 KO cells.

RNA-sequencing analysis

According to manufacturer's recommendation, TruSeq Stranded mRNA Library Prep Kit (Illumina, San Diego, CA, USA) was used to the stable vector and SIK3 overexpression MDA-MB-231 cell-purified RNA to prepare the sequencing library. After the double-stranded cDNA is generated and adenylated at the 3′ end of the DNA fragment, the adaptor is ligated and purified using the AMPure XP system (Beckman Coulter, Miami, USA). The library quality was evaluated on the Agilent Bioanalyzer 2100 system and real-time PCR system. Then the qualified library was sequenced on the Illumina NovaSeq 6000 platform, and 150 bp paired-end reads were generated by Genomics, BioSci & Tech Co. (New Taipei City, Taiwan). The RNA expression level of each gene was expressed as a log 2 fragments per kilobase million (FPKM) value. Genes were selected based on functions related to the cell cycle, cell growth, proliferation, drug resistance, and metastasis. Genes that were significantly different between 231-Vc and 231-SIK3 cells were determined by increasing or decreasing the expression level of log2 transcripts. GSEA and heatmap analysis follows standard procedures (https://www.gsea-msigdb.org/gsea/index.jsp), the selected hallmark gene sets of the molecular signature database used by the GSEA user guide was used to calculate the overlap signature between our gene set and the gene set in the molecule database.

Transwell migration assay

The cells (231-Vc and 231-SIK3) were seeded with 2×10^4 cells in the upper chamber of a Transwell containing DMEM/F12 medium without FBS and Matrigel. The Transwell was inserted into 24-well plates containing 500 uL of 10% FBS DMEM/F12 medium. The plate was incubated with 5% CO_2 in a 37 °C incubator for 16 h. After the incubation period, the cells migrated to the undersurface of the membrane of the Transwell. The membrane was washed three times with PBS, fixed with 4% formaldehyde (Sigma–Aldrich, St. Louis, MO, USA), stained with 0.05% crystal violet, and observed. The Leica DM500 Microscope Imaging System (Leica Microsystems, Wetzlar, Germany) captured images in a high power field (HPF) through a microscope. Three replicate samples were used for each cell line type.

Flowcytometric analysis

SK-Vc (n = 2) and SK-SIK3 cells (n = 2) were treated with media supplemented with 0.04% FBS for 48 h to synchronize their cell cycle statuses and then incubated with a fresh medium containing 10% FBS in a time-dependent manner (0, 6, 12, 18, and 24 h). BD FACScaliber cytometer (Becton Dickinson, Sunnyvale, CA, USA) was used to obtain flow cytometric data (10000 events), and Cell Quest Pro software (Becton Dickinson, Sunnyvale, CA, USA) was utilized to determine the percentage of cells in each cell cycle phase.

Western blotting assay

To evaluate the protein expression of SIK3, cell cycle, and migration-related proteins, cells were lysed in ice in Golden lysis buffer (20 mM Tris–HCl, pH 8.0, 137 mM NaCl, 5 mM EDTA, 5 mM EGTA, 10 mM NaF, 1% Triton X-100, and 10% glycerol) containing protease inhibitors. The protein lysates were loaded into 12% sodium dodecyl sulfate-polyacrylamide gel electrophoresis and transferred to nitrocellulose paper (Millipore, Billerica, MA, USA). The membranes were incubated with 5% fat-free milk for 1 h, the primary antibodies overnight, and secondary antibodies for 1 h. The western blots were analyzed, and the image was captured using the UVP BioSpectrum 500 Imaging System (Thermo Fisher Scientific, Waltham, MA, USA).

Immunohistochemistry (IHC) stain

The tumor samples were harvested from PDX mice. The standard protocol for the IHC procedure is as follows: paraffin tissue sections were incubated at 60 °C for 1 h and then deparaffinized with xylene. The tumor sections were rehydrated with graded ethanol (twice every 30 s), heated in Tris–EDTA (pH 9.0) buffer for 30 min to recover the antigen, and then transferred to 3% hydrogen peroxide in methanol for 10 min. The sections were incubated with 10% FBS for 30 min, primary antibodies (1:100) for 4 h, and secondary antibodies for 30 min. The liquid DAB-Substrate Chromogen System (K3468, Dako, Carpinteria, CA, USA) was used for

immunostaining, resulted in the staining of antigen site as brown precipitates. It was then counterstained with hematoxylin and then dehydrated. The sections were mounted with a non-aqueous mounting medium.

TUNEL assay

Apoptotic cells in PDX tumors were detected according to the protocol of DeadEnd Colorimetric TUNEL Assay System (Promega, Madison, WI, USA). The protocol of the TUNEL system is as follows: paraffin tissue sections were incubated at 60 °C for 1 h and then deparaffinized twice with xylene. The sections were rehydrated with graded ethanol (twice every 30 s), washed with 0.8% of NaCl for 5 min, and then immersed in PBS for 5 min. Afterward, the sections were fixed with 4% paraformaldehyde in PBS for 15 min and washed twice with PBS for 5 min each time. Then the sections were incubated with 100 μL 20 μg/mL proteinase K solution at room temperature for 10–30 min and washed with PBS for 5 min to infiltrate the slides of the tissue section. Subsequently, the sections were re-fixed with 4% paraformaldehyde in PBS for 5 min and were incubated in 100 μL equilibration buffer for 5–10 min at room temperature, labeled with 100 μL TdT reaction mixture, and further incubated at 37 °C for 60 min. Finally, the sections were immersed in 2X SSC for 15 min to stop the reaction, incubated with 0.3% hydrogen peroxide for 3–5 min, and stained with 100 μL DAB solution (100 μL DAB 10x Chromogen plus 900 μL DAB substrate 1x Buffer). The sections were mounted with a non-aqueous mounting medium.

Table S1. Primers used for qPCR.

Gene	Sequence	Product size (bp)
SIK3	F: 5′- TCAGCAGCAACCTGAGAACT	251
	R: 5′- ACAAGGGACGGTGCCCATAG	
GUS	F: 5′- AAACAGCCCGTTTACTTGAG	166
	R: 5′- AGTGTTCCCTGCTAGAATAGATG	

References

[1] Harbeck N, Penault-Llorca F, Cortes J, Gnant M, Houssami N, Poortmans P, et al. Nat Rev Dis Primers 2019;5:66.

[2] Bianchini G, Balko JM, Mayer IA, Sanders ME, Gianni L. Triple-negative breast cancer: challenges and opportunities of a heterogeneous disease. Nat Rev Clin Oncol 2016;13:674–90.

[3] Kong WY, Ngai SC, Goh BH, Lee LH, Htar TT, Chuah LH. Is curcumin the answer to future chemotherapy cocktail? Molecules 2021:26.

[4] Farghadani R, Naidu R. Curcumin: modulator of key molecular signaling pathways in hormone-independent breast cancer. Cancers 2021;13.

[5] Gadag S, Narayan R, Nayak AS, Catalina Ardila D, Sant S, Nayak Y, et al. Development and preclinical evaluation of microneedle-assisted resveratrol loaded nanostructured lipid carriers for localized delivery to breast cancer therapy. Int J Pharm 2021;606:120877.

[6] Deng L, Wu X, Zhu X, Yu Z, Liu Z, Wang J, et al. Combination effect of curcumin with docetaxel on the PI3K/AKT/mTOR pathway to induce autophagy and apoptosis in esophageal squamous cell carcinoma. Am J Transl Res 2021;13:57–72.

[7] Saghatelyan T, Tananyan A, Janoyan N, Tadevosyan A, Petrosyan H, Hovhannisyan A, et al. Efficacy and safety of curcumin in combination with paclitaxel in patients with advanced, metastatic breast cancer: a comparative, randomized, double-blind, placebo-controlled clinical trial. Phytomedicine 2020;70:153218.

[8] Kashyap D, Garg VK, Sandberg EN, Goel N, Bishayee A. Oncogenic and tumor suppressive components of the cell cycle in breast cancer progression and prognosis. Pharmaceutics 2021:13.

[9] Hu Y, Gao J, Wang M, Li M. Potential prospect of CDK4/6 inhibitors in triple-negative breast cancer. Canc Manag Res 2021;13:5223–37.

[10] Hui R, de Boer R, Lim E, Yeo B, Lynch J. CDK4/6 inhibitor plus endocrine therapy for hormone receptor-positive, HER2-negative metastatic breast cancer: the new standard of care. Asia Pac J Clin Oncol 2021;17(Suppl 1):3–14.

[11] Roy A, Banerjee S. p27 and leukemia: cell cycle and beyond. J Cell Physiol 2015;230:504–9.

[12] Porter PL, Barlow WE, Yeh IT, Lin MG, Yuan XP, Donato E, et al. p27(Kip1) and cyclin E expression and breast cancer survival after treatment with adjuvant chemotherapy. J Natl Cancer Inst 2006;98:1723–31.

[13] Sun Z, Jiang Q, Li J, Guo J. The potent roles of salt-inducible kinases (SIKs) in metabolic homeostasis and tumorigenesis. Signal Transduct Target Ther 2020;5:150.

[14] Chen F, Chen L, Qin Q, Sun X. Salt-Inducible kinase 2: an oncogenic signal transmitter and potential target for cancer therapy. Front Oncol 2019;9:18.

[15] Murray CW, Brady JJ, Tsai MK, Li C, Winters IP, Tang R, et al. An LKB1-SIK Axis suppresses lung tumor growth and controls differentiation. Canc Discov 2019;9:1590–605.

[16] Amara S, Majors C, Roy B, Hill S, Rose KL, Myles EL, et al. Critical role of SIK3 in mediating high salt and IL-17 synergy leading to breast cancer cell proliferation. PloS One 2017;12:e0180097.

[17] Bon H, Wadhwa K, Schreiner A, Osborne M, Carroll T, Ramos-Montoya A, et al. Salt-inducible kinase 2 regulates mitotic progression and transcription in prostate cancer. Mol Canc Res 2015;13:620–35.

[18] Charoenfuprasert S, Yang YY, Lee YC, Chao KC, Chu PY, Lai CR, et al. Identification of salt-inducible kinase 3 as a novel tumor antigen associated with tumorigenesis of ovarian cancer. Oncogene 2011;30:3570–84.

[19] Du WQ, Zheng JN, Pei DS. The diverse oncogenic and tumor suppressor roles of salt-inducible kinase (SIK) in cancer. Expert Opin Ther Targets 2016;20:477–85.

[20] Lee CH, Huang CS, Chen CS, Tu SH, Wang YJ, Chang YJ, et al. Overexpression and activation of the alpha9-nicotinic receptor during tumorigenesis in human breast epithelial cells. J Natl Cancer Inst 2010;102:1322–35.

[21] Lin CY, Lee CH, Chuang YH, Lee JY, Chiu YY, Wu Lee YH, et al. Membrane protein-regulated networks across human cancers. Nat Commun 2019;10:3131.

[22] Lin CY, Tsai PH, Kandaswami CC, Lee PP, Huang CJ, Hwang JJ, et al. Matrix metalloproteinase-9 cooperates with transcription factor Snail to induce epithelial-mesenchymal transition. Canc Sci 2011;102:815–27.

[23] Kalluri R, Weinberg RA. The basics of epithelial-mesenchymal transition. J Clin Invest 2009;119:1420–8.

[24] Huang CS, Ho WL, Lee WS, Sheu MT, Wang YJ, Tu SH, et al. SP1-regulated p27/Kip1 gene expression is involved in terbinafine-induced human A431 cancer cell differentiation: an in vitro and in vivo study. Biochem Pharmacol 2008;75:1783–96.

[25] Xiong K, Zhang Y, Wen Q, Luo J, Lu Y, Wu Z, et al. Co-delivery of paclitaxel and curcumin by biodegradable polymeric nanoparticles for breast cancer chemotherapy. Int J Pharm 2020;589:119875.
[26] Howells LM, Iwuji COO, Irving GRB, Barber S, Walter H, Sidat Z, et al. Curcumin combined with FOLFOX chemotherapy is Safe and tolerable in patients with metastatic colorectal cancer in a randomized phase IIa trial. J Nutr 2019; 149:1133−9.
[27] Moballegh Nasery M, Abadi B, Poormoghadam D, Zarrabi A, Keyhanvar P, Khanbabaei H, et al. Curcumin delivery mediated by bio-based nanoparticles: a Review. Molecules 2020;25.
[28] Prasad S, DuBourdieu D, Srivastava A, Kumar P, Lall R. Metal-curcumin complexes in therapeutics: an approach to enhance pharmacological effects of curcumin. Int J Mol Sci 2021:22.
[29] Liu Y, Wang X, Zeng S, Zhang X, Zhao J, Zhang X, et al. The natural polyphenol curcumin induces apoptosis by suppressing STAT3 signaling in esophageal squamous cell carcinoma. J Exp Clin Canc Res 2018;37:303.
[30] Debata PR, Begum S, Mata A, Genzer O, Kleiner MJ, Banerjee P, et al. Curcumin potentiates the ability of sunitinib to eliminate the VHL-lacking renal cancer cells 786-O: rapid inhibition of Rb phosphorylation as a preamble to cyclin D1 inhibition. Anticancer Agents Med Chem 2013;13: 1508−13.
[31] Zhu X, Mulcahy LA, Mohammed RA, Lee AH, Franks HA, Kilpatrick L, et al. IL-17 expression by breast-cancer-associated macrophages: IL-17 promotes invasiveness of breast cancer cell lines. Breast Cancer Res 2008;10:R95.
[32] Wang HC, Lee WS. Molecular mechanisms underlying progesterone-induced cytoplasmic retention of p27 in breast cancer cells. J Steroid Biochem Mol Biol 2018;183:202−9.
[33] Guiley KZ, Stevenson JW, Lou K, Barkovich KJ, Kumarasamy V, Wijeratne TU, et al. p27 allosterically activates cyclin-dependent kinase 4 and antagonizes palbociclib inhibition. Science 2019:366.